STEM CELLS AND DEVELOPMENT
Volume 24, Number 10, 2015

DOI: 10.1089/scd.2014.0293

Multi-Drug Resistance ABC Transporter Inhibition Enhances Murine Ventral Prostate Stem/Progenitor Cell Differentiation

Mugdha D. Samant,[1] Courtney M. Jackson,[1,*] Carina L. Felix,[2] Anthony J. Jones,[1,†] David W. Goodrich,[1] Barbara A. Foster,[1] and Wendy J. Huss[1,3]

Multi-drug resistance (MDR)-ATP binding cassette (ABC) transporters, ABCB1, ABCC1, and ABCG2 participate in the efflux of steroid hormones, estrogens, and androgens, which regulate prostate development and differentiation. The role of MDR-ABC efflux transporters in prostate epithelial proliferation and differentiation remains unclear. We hypothesized that MDR-ABC transporters regulate prostate differentiation and epithelium regeneration. Prostate epithelial differentiation was studied using histology, sphere formation assay, and prostate regeneration induced by cycles of repeated androgen withdrawal and replacement. Embryonic deletion of *Abcg2* resulted in a decreased number of luminal cells in the prostate and increased sphere formation efficiency, indicating an imbalance in the prostate epithelial differentiation pattern. Decreased luminal cell number in the Abcg2 null prostate implies reduced differentiation. Enhanced sphere formation efficiency in Abcg2 null prostate cells implies activation of the stem/progenitor cells. Prostate regeneration was associated with profound activation of the stem/progenitor cells, indicating the role of Abcg2 in maintaining stem/progenitor cell pool. Since embryonic deletion of *Abcg2* may result in compensation by other ABC transporters, pharmacological inhibition of MDR-ABC efflux was performed. Pharmacological inhibition of MDR-ABC efflux enhanced prostate epithelial differentiation in sphere culture and during prostate regeneration. In conclusion, *Abcg2* deletion leads to activation of the stem/progenitor cells and enhances differentiating divisions; and pharmacological inhibition of MDR-ABC efflux leads to epithelial differentiation. Our study demonstrates for the first time that MDR-ABC efflux transporter inhibition results in enhanced prostate epithelial cell differentiation.

Introduction

Prenatal and postnatal murine prostate development has been extensively studied to understand the prostate epithelial differentiation hierarchy and signaling pathways involved in the developing prostate [1]. One theory of prostate epithelial differentiation is that basal and luminal cells differentiate from adult stem cells [2]. Classic androgen deprivation and regeneration studies demonstrated that adult stem cells are present in the basal layer of the prostate gland [3–5]. However, the latest lineage tracing experiments during murine postnatal prostate development suggest that stem/progenitor cells are present in both basal and luminal cell compartments [6–10]. Multi-drug resistance-ATP binding cassette (MDR-ABC) transporters potentially regulate prostate epithelial differentiation by mediating efflux of steroids [11,12]. In low-calcium, serum-free media, human prostate cells expressing stem cell markers CD133 and ABCG2 generate $CD133^-/ABCG2^-$ transit amplifying and neuroendocrine cells, indicating that CD133 and ABCG2 expressing cells can differentiate into multiple lineages [13]. Moreover, transcriptome profiling of human prostate ABCG2+cells showed stem cell gene expression pattern [14]. Previous findings from our lab also suggest that the ABC transporter efflux assay enriches for human prostate stem cells [15].

Studies using MDR-ABC transporter embryonic knockout mice do not validate an absolute necessity for specific ABC transporter in the maintenance of the normal stem cell compartment, and mice lacking *Abcb1* and *Abcg2* expression develop minor defects [16]. Therefore, ABC transporter genes are not individually responsible for stem cell maintenance. Functional redundancy of ABC transporters possibly diminishes their importance in stem cell maintenance. However, studies in the *Abcg2* knockout mouse model

Departments of [1]Pharmacology and Therapeutics and [3]Urologic Oncology, Roswell Park Cancer Institute, Buffalo, New York.
[2]Department of Biology, Howard University, Washington, District of Columbia.
*Current affiliation: Immunobiology Graduate Program, Cincinnati Children's Hospital, University of Cincinnati, Cincinnati, Ohio.
†Current affiliation: Department of Pharmacology and Toxicology, State University of New York at Buffalo, Buffalo, New York.

indicate a critical role of Abcg2 in the epithelial stem cell and endothelial compartments during replenishment of injured tissue [17,18].

In contrast to the studies with MDR-ABC transporter knockout mice, over-expression studies implicate MDR-ABC transporters with stem cell expansion. For example, in mouse bone marrow cells, enforced *Abcb1* expression leads to dramatic ex vivo stem cell expansion and myeloproliferative disorder after engraftment [19]. Moreover, enforced expression of *Abcg2* in bone marrow cells causes a reduction in the mature progeny both in vivo and in vitro [20]. Reduction in the mature progeny in bone marrow indicates that high expression of MDR-ABC transporters may amplify stem cells, as in cancer or regeneration after injury. Oncogenes, such as *cMyc* cause up-regulation of ABC transporter expression, leading to drug resistance by effluxing an array of chemotherapeutic agents [21]. Hence, the super-family of ABC transporters is well characterized for MDR in cancer cells. The best-known and studied transporters for MDR in human cancers are ABCB1, ABCC1, and ABCG2. This study determines the role of the mouse MDR-ABC transporter homologues (*Abcb1*, *Abcc1*, and *Abcg2*) in the prostate. The MDR-ABC transporter inhibitors have been intensively studied for three decades and have been used in clinical trials to avoid drug resistance in cancer. However, the first-generation MDR-ABC transporter inhibitors failed in clinical trials because of toxicities [22]. The third-generation MDR-ABC transporter inhibitors are more potent, highly specific, not substrates of MDR-ABC transporters, and in various stages of clinical trials [22].

Apart from the function in chemoresistance, MDR-ABC transporters may play a role in regulating steroid hormone-mediated differentiation of prostate epithelium. Studies show that MDR-ABC transporters, ABCB1 and ABCG2 are involved in steroid efflux, for example, dihydrotestosterone (DHT) in prostate cell lines [11,12]. Proliferation and differentiation of embryonic and adult prostate epithelial cells are highly dependent on endocrine hormones such as estrogens and androgens [1]. In this study, we investigated the hypothesis that inhibition of MDR-ABC transporter function impairs the differentiation pattern of prostate epithelium.

In both mouse and human adult prostate glands, the three main epithelial cell types are cuboidal and secretory luminal cells, which express cytokeratins (CK) 8 and 18; basal cells that express CK5, CK14, and p63; and rare neuroendocrine cells, expressing synaptophysin and chromogranin A. Both the mouse and human prostates have similar glands and ducts; however, there are significant differences between the stromal components. The human prostate has robust fibromuscular stroma, while the mouse prostate has a very modest stromal component [23]. The mouse dorsolateral prostate is considered analogous to the human peripheral zone [23]. However, the mouse ventral prostate does not have a human homologue. Historically, testosterone action was studied mainly in rat ventral prostate [24–26]. In this study, the differentiation pattern of the ventral prostate was examined, as the ventral prostate epithelium is the least convoluted (Supplementary Fig. S1; Supplementary Data are available online at www.liebertpub.com/scd) and the defect in epithelial differentiation is prominent in ventral prostate (Fig. 1B–D). Moreover, the androgen responsiveness in terms of apoptotic cell death after androgen deprivation is pronounced in the ventral prostate compared with the dorsolateral prostate [27].

For the purpose of this study, the Abcg2 null mouse model was used to demonstrate the MDR-ABC transporter function in prostate epithelial differentiation. Reversan, a third-generation inhibitor, was used to inhibit MDR-ABC transporters [22] in wild-type (WT) and Abcg2 null mouse prostates. Based on previous studies [12,14,15,28], the absence of *Abcg2* was predicted to impair the pattern of prostate epithelial differentiation, and with inhibition of the MDR-ABC transporters the differentiation pattern disruption was more profound.

Materials and Methods

Mice

Abcg2 null mice with exons 3 and 4 deleted were obtained from Dr. Brian Sorrentino (St. Jude Children's Research Hospital, Memphis, TN) [29]. $Abcg2^{-/-}$ male and female mice with a mixed background of C57BL/6 and 129/Ola were bred in the Roswell Park Cancer Institute (RPCI) animal facility according to an institutional animal care and use committee (IACUC) approved protocol. WT mice with the background C57BL/6 were ordered from Taconic Laboratories, Hudson, New York and used as controls. Serum testosterone levels of WT and Abcg2 null mice were determined by radioimmunoassay at the Animal Health Diagnostic Center at Cornell University, Ithaca, New York.

Immunohistochemistry

Prostates or spheres were embedded in paraffin. Serial sections (5 μm) were cut on a microtome (Leica Microsystems) and mounted on glass slides (Fisherbrand probe on plus, Fisher Scientific, 22-230-900). Slides were deparaffinized in xylene, rehydrated through a graded series of alcohol washes, and equilibrated in phosphate-buffered saline (PBS). Antigen retrieval was performed in 10 mM citric acid, pH 6.0 for 30 min in a steamer. Slides were incubated with appropriate primary antibodies, diluted in PBS with 5% goat serum (Vector Laboratories, Inc.): 1:50 dilution of mouse monoclonal anti-p63 clone 4A4 (Santa Cruz; sc-8431); 1:50 dilution of rat monoclonal anti-Abcg2 clone Bxp53 (Abcam; ab24115), and 1:500 dilution of rabbit polyclonal anti-Ki67 (Leica Biosystems; NCL-Ki67p) for 30 min at 37°C. All slides were incubated with the appropriate biotinylated secondary antibody, diluted in PBS with 5% goat serum: 1:1,000 dilution goat anti-mouse IgG (Vector Laboratories, Inc.; BA9200) or 1:1,000 dilution goat anti-rat IgG (Vector Laboratories, Inc.; BA4000) or 1:1,000 dilution goat anti-rabbit IgG (Vector Laboratories, Inc.; BA1000) for 20 min at 37°C. Immunoreactive antigens were detected using streptavidin (Vector Laboratories, Inc.; SA5704) and diaminobenzidine (Life Technologies; D22187).

Immunohistochemistry image analysis

Each ventral prostate specimen immunostained for p63 was scanned using Aperio Imagescope at 40× magnification. For each prostate histological section, images were acquired from 10 to 15 representative sites. The number of luminal epithelial cells and p63-positive basal epithelial cells was

quantitated in mouse prostate ducts cross-sections; longitudinal cuts were excluded from analysis. The least convoluted ducts were selected from the proximal prostate (Supplementary Fig. S1). In this study, we defined luminal epithelial cells as p63-negative columnar cells adjacent to the lumen, with abundant cytoplasm and round nuclei, whereas basal epithelial cells were defined as triangular-shaped p63-positive cells, with little cytoplasm [30].

Androgen cycling and reversan treatment

Male Abcg2 null mice and C57BL/6 WT mice were castrated at 8–12 weeks of age through a scrotal incision under isoflurane-anesthesia. For androgen cycling experiments, castrated mice were subcutaneously implanted with silastic tubing (Dow Corning; 2415569) packed with 10-mg testosterone powder (Sigma; T1500) on day 14 postcastration. Prostate regeneration was analyzed after 7 days of testosterone administration. Fourteen days of castration followed by 7 days of testosterone administration constitute one cycle of regression and regeneration. Ventral prostates were examined after one cycle and five cycles of castration and testosterone replacement for changes in the basal and luminal cell compartments. Ventral prostates were microdissected and collected for immunohistochemistry analysis or digested for sphere formation analysis. Animals in the reversan treatment group were treated with 10 mg/kg reversan in DMSO (Corning; 25-950-CQC), injected once a day, intraperitoneally for 5 days, starting at the time of testosterone replacement. Animals in the control group were treated with DMSO. Mice were sacrificed at 6 h after the last reversan injection. Ventral prostates were micro-dissected and processed for immunohistochemistry.

Sphere formation assay

The sphere formation assay was performed according to a published protocol [31]. Briefly, ventral prostates were digested using 1 mg/mL of collagenase (Life Technologies; 17100-017) at 37°C for 3 h, while shaking at 120 rpm. Prostate cells were resuspended in PrEGM media (Lonza; CC-3166). 1–5×10^5 cells were added to each well of 24-well ultra-low attachment plates (Corning; 3473). The cells were uniformly distributed along the rim of the well by rotating the plate. Matrigel (60 μL) (BD Biosciences; 354,234) was added and mixed with the cell suspension. Matrigel was allowed to solidify at 37°C for 30 min and then covered with 800 μL of PrEGM media. The spheres were grown at 37°C at 5% CO_2 levels. For the reversan treatment experiments, spheres were treated with either 1 or 5 μM reversan (Sigma; SML0173) or DMSO (Corning; 25-950-CQC) as a vehicle control for 10–14 days. Abcg2 was inhibited in the sphere culture with 5 μM Ko143 (Sigma; K2144). The media was changed every 3 days. Spheres were counted after 7–14 days. Images of spheres were captured using an Olympus inverted microscope attached with a SPOT, RT Slider, Diagnostic Instruments camera. Size measurements were performed using SPOT basic software.

Immunofluorescence microscopy for spheres

Spheres were collected after 7 and 14 days by centrifugation and mixed with 20 μL of histogel (Thermo Scientific; HG-400-012). Histogel was allowed to solidify and was embedded in paraffin. Serial sections were cut as described earlier. Slides were deparaffinized in xylene, rehydrated through a graded series of alcohol washes, and equilibrated in PBS. Slides were permeabilized using 0.1% Triton X-100 in PBS for 45 min at room temperature and blocked with 2% bovine serum albumin (BSA) in PBS for 1 h at room temperature. All slides were incubated at room temperature for 1 h with appropriate primary antibodies: 1:1,000 dilution of rabbit polyclonal anti-CK5 (Covance; PRB-160P-100), 1:1,000 dilution of mouse monoclonal anti-CK8, clone 1E8 (Covance; MMS-1602P-250), and 1:1,000 dilution of mouse monoclonal anti-p63 clone 4A4 (Santa Cruz; sc-8431). After washing slides with PBS thrice, all slides were incubated for 1 h at room temperature with appropriate secondary antibody in 2% BSA in PBS: 1:1,000 dilution of Alexa Fluor 488 donkey anti-rabbit IgG (Life Technologies; A21206), 1:1,000 dilution of Alexa Fluor 594 goat anti-mouse IgG (Life Technologies; A11005). Slides were then washed thrice with PBS, mounted using Vectashield with DAPI (Vector Laboratories, Inc.; H1200), and covered with coverslips.

mRNA extraction and quantitative reverse transcription-PCR

Spheres were lysed using 1 mL of Trizol (Ambion; 15596-026) by sonication. RNA was isolated according to the manufacturer's instructions. RNA was quantitated using Nanodrop 8000 (Thermo Scientific). RNA (100–500 ng) was reverse transcribed using a first-strand cDNA synthesis kit (Invitrogen; 18080-051). SyberGreen (Applied Biosystems; 4309155) chemistry was used for quantitative reverse transcription-PCR (qRT-PCR). The following primers were used: CK5 forward primer: 5′-ACCTTCGAA ACACCAAGCAC-3′, CK5 reverse primer: 5′-TTGGCACA CTGCTTCTTGAC-3′, CK8 forward primer: 5′-ATCGAGA TCACCACCTACCG-3′, CK8 reverse primer: 5′-TGAAGC CAGGGCTAGTGAGT-3′, p63 forward primer: 5′-GAAGG CAGATGAAGACAGCA-3′, p63 reverse primer: 5′-GGAA GTCATCTGGATTCCGT-3′, GAPDH forward primer: 5′-GGGTGTGAACCACGAG AAAT-3′, GAPDH reverse primer: 5′-ACACATTGGGGG TAGGAACA-3′. For qRT-PCR analysis, 7300 real-time PCR system (Applied Biosystems) was used. Each reaction was performed in triplicate. The expression of CK5, CK8, and p63 mRNA was normalized to endogenous GAPDH mRNA levels. The fold change in mRNA expression levels of spheres generated by WT and Abcg2 null prostate cells was normalized to spheres generated by WT prostate cells at day 10. In the case of reversan and Ko143 treatments, the mRNA expression levels of inhibitor-treated spheres were normalized to mRNA expression levels of spheres generated from WT prostate cells at day 10 treated with vehicle control.

Side population assay

The side population assay was performed using 1×10^6 cells/mL of HANKS (Life Technologies, Gibco; 14025-076) buffer with 1% fetal bovine serum in 15 mL polypropylene tubes. The cells were preincubated for 15 min with 1 μM reversan (Sigma; SML0173) to inhibit MDR-ABC efflux pumps. Hoechst-33342 dye (Life Technologies; H1399) at a final concentration of 5 μg/mL was added to cells that were preincubated with or without inhibitor and incubated for

90 min at 37°C, with intermittent vortexing. The cells were further stained with FITC-conjugated antibodies against the following lineage markers: CD31 (eBioscience; 11-0311), CD45 (eBioscience; 11-0451), Ter119 (eBioscience; 11-5921), PeCy7 conjugated anti-Stem cell antigen (Sca) antibody (eBioscience; 25-5981), and APC-Efluor788 conjugated anti-CD44 antibody (eBioscience; 47-0441). Single-color controls were used to set compensation. Side population analysis was performed using BD FACS LSRII, as described [32,33]. Briefly, UV laser (351 nm) at the power 100 mW was used. Hoechst fluorescence was analyzed using 450/50 (blue) and 645 LP (red) filter sets. The debris and clumps of cells were gated out based on forward scatter and side scatter. The gate was applied on the side population that was eliminated with reversan.

Statistics

All graphs were plotted, and statistical analysis was performed using GraphPadPrism software, version 6. *P* values for comparisons of two groups were calculated using Student's *t* test. For comparisons of more than two groups, *P* values were calculated using two-way ANOVA with multiple *t* tests. The error bars represent standard errors from the mean.

Results

Luminal cell number is decreased in Abcg2 null ventral prostate, and androgen cycling normalizes the Abcg2 null luminal cell compartment

To elucidate the effect of *Abcg2* deletion on the prostate luminal cell compartment, the number and luminal cell morphology were determined in intact Abcg2 null ventral prostates compared with WT ventral prostates. Ventral prostate luminal and basal cells were counted in WT and Abcg2 null mouse prostate ducts cross-sections. The least convoluted ducts were selected from the proximal prostate (Supplementary Fig. S1). The number of p63-negative columnar luminal cells/perimeter length of ventral prostate was significantly reduced in Abcg2 null prostates as compared with WT controls ($P < 0.001$) (Fig. 1A). No profound alteration was found in basal cell numbers in prostates from the two genotypes (Fig. 1A). Histologically, in the cross-sectional plane of the prostate ducts, the luminal cell nuclei of the Abcg2 null ventral prostate were less tightly packed, rounder and smaller (Fig. 1C) compared with the luminal cell nuclei of the WT ventral prostate (Fig. 1B). Moreover, the luminal cells of Abcg2 null ventral prostate showed cuboidal morphology, as compared with the tall columnar structure of the luminal cells of WT ventral prostate (Fig. 1D). Flow cytometry analysis was performed to measure the number of $Lin^-Sca^{High}CD44^{High}$ basal cells and Lin^- Sca^{Low} $CD44^{Low}$ luminal cells in WT (Fig. 1E) and Abcg2 null ventral prostates (Fig. 1F). Flow cytometry analysis demonstrated that 20.7% of cells were Lin^- $Sca^{Low}CD44^{Low}$ in Abcg2 null ventral prostate (Fig. 1F) compared with 33.4% of cells that were Lin^- $Sca^{Low}CD44^{Low}$ in WT controls (Fig. 1E), displaying $\sim$13% reduction in Abcg2 null ventral prostate luminal cells. However, percentages of Lin^-Sca^{High} $CD44^{High}$ basal cells did not show a profound difference (Fig. 1E, F), confirming that the decrease in luminal cells was not accompanied by an alteration in the number of basal or stem/progenitor cell population.

Previous findings demonstrated that serum testosterone levels were reduced when *Abcc1* and *Abcc4* transporters were knocked out embryonically [34,35]. Based on these previous findings, we hypothesized that the reduction in the luminal cell number is due to altered testosterone levels and/or homeostasis. Hence, the serum testosterone levels of WT and Abcg2 null mice were compared. There was no difference in serum testosterone levels between Abcg2 null mice as compared with WT mice ($P = 0.84$) (Fig. 1G). However, the serum testosterone levels in WT and Abcg2 null mice were highly variable. To understand the effect of variable testosterone levels on Abcg2 null prostates, castration and androgen replacement was performed. Castration and androgen replacement normalizes serum testosterone levels in WT and Abcg2 null mice. The prostate luminal cell compartment was analyzed after castration (regression) and androgen stimulation (regeneration) (Fig. 1H). The luminal cells/ventral prostate gland did not show a difference after regression and regeneration in Abcg2 null mice compared with WT controls (Fig. 1I), indicating that replacement of testosterone normalized the testosterone levels in both WT and Abcg2 null mice and eliminated the difference between

FIG. 1. The differentiation pattern of Abcg2 null mouse ventral prostate is altered. **(A)** Quantitation of $p63^+$ basal cells and $p63^-$ luminal cells in WT ($n = 3$) and Abcg2 null ($n = 3$) ventral prostate sections immunostained for p63. ($P = 0.13$, basal cells; $P < 0.001$, luminal cells calculated using Student's *t* test). Quantitation was performed on images captured from 20 representative sites, 6–7 from each mouse. Each point represents number of cells/perimeter length in arbitrary units of prostate basement membrane. **(B)** Immunohistochemistry staining for p63 of cross-sectional plain of a WT prostate duct and **(C)** Abcg2 null ventral prostate duct at the age of 10 weeks, bar = 50 μm. **(D)** Magnified areas from **(B)** and **(C)** showing tall columnar luminal cells in WT ventral prostate while cuboidal Abcg2 null luminal cells with less cytoplasm, bar = 50 μm. Flow cytometry analysis of **(E)** WT ($n = 4$ pooled ventral prostates) and **(F)** Abcg2 null ($n = 4$ pooled ventral prostates) ventral prostate cells showing $Lin^-Sca^{high}CD44^{high}$ basal and $Lin^-Sca^{low}CD44^{low}$ luminal cells. The percentages represent the specific cell population within Lin^- cells. **(G)** Serum testosterone levels of WT ($n = 18$) and Abcg2 null mice ($n = 20$) in ng/mL ($P = 0.84$, calculated using Student's *t* test). **(H)** Schematic representation of prostate regression and regeneration followed by androgen deprivation (Cx) and replacement (+T) for one and five cycles. **(I)** Quantitation of $p63^-$ luminal cells in WT ($n = 3$) and Abcg2 null ($n = 3$) ventral prostate sections immunostained for p63. Quantitation was performed on images captured from 7 to 10 representative prostate ducts, 2–3 ducts from each mouse. Each point represents number of cells/prostate gland (Intact, $P < 0.001$; one cycle Cx, $P = 0.59$, one cycle Cx + T, $P = 0.27$; 5 cycle Cx, $P = 0.1$; five cycles Cx + T, $P = 0.49$; calculated using Student's *t* tests). Flow cytometry analysis of **(J)** WT ($n = 4$ pooled ventral prostates) and **(K)** Abcg2 null ($n = 4$ pooled ventral prostates) ventral prostate cells after one cycle of androgen deprivation and replacement (Cx + T) showing $Lin^-Sca^{high}CD44^{high}$ basal and Lin^- $Sca^{low}CD44^{low}$ luminal cells. Color images available online at www.liebertpub.com/scd

the luminal cell numbers/prostate glands. Further analysis of luminal cells was performed using flow cytometry. Flow cytometry analysis after one cycle of regression and regeneration demonstrated ~6% difference between Lin^- $Sca^{Low}CD44^{Low}$ luminal cells in Abcg2 null ventral prostates (24.0%) (Fig. 1K) compared with WT controls (30.5%) (Fig. 1J). The difference between Lin^- $Sca^{Low}CD44^{Low}$cells of WT and Abcg2 null ventral prostates decreased from 13% in intact mouse prostates (33.4% in WT to 20.7% in Abcg2 null) (Fig. 1E, F) to 6% after regeneration (30.5% in WT to 24% in Abcg2 null) (Fig. 1J, K). Thus testosterone replacement resulted in considerable normalization in the

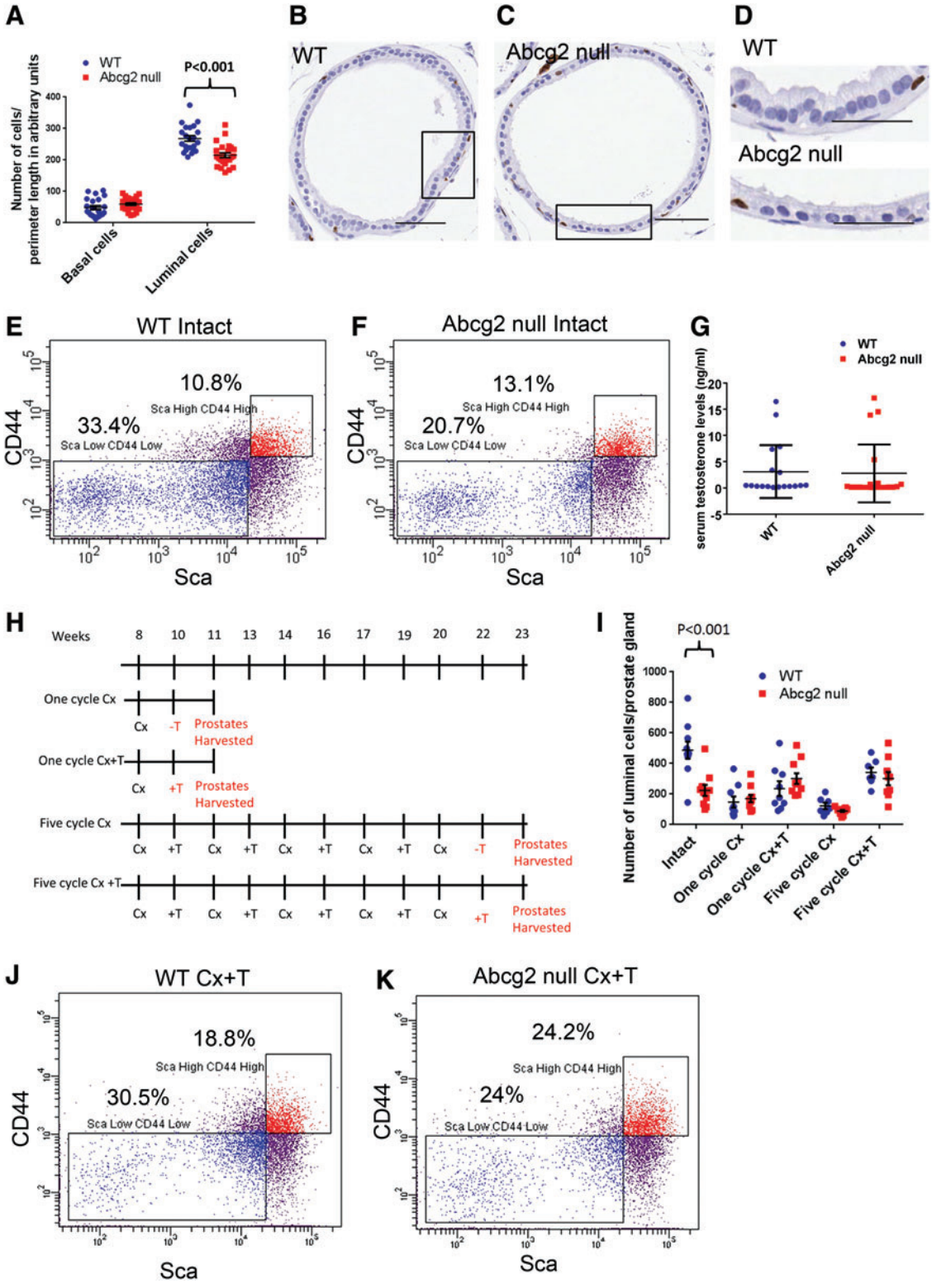

luminal cell compartment. However, the difference between $Lin^{-}Sca^{High}CD44^{High}$ basal cells of WT and Abcg2 null ventral prostates changed from 3% in intact mouse prostates (10.8% in WT to 13.1% in Abcg2 null) (Fig. 1E, F) to 6% after regeneration (18.8% in WT to 24.2% in Abcg2 null) (Fig. 1J, K), suggesting no significant difference in the number of basal cells in Abcg2 null ventral prostates after regression and regeneration. These data indicate that androgen cycling normalizes the luminal cell compartment of Abcg2 null prostate with no significant alteration in the basal cell compartment, suggesting that the reduced luminal cell number is a result of altered testosterone homeostasis.

Sphere formation efficiency is highly enhanced in Abcg2 null prostate cells

Since Abcg2 is expressed in a small fraction of non-luminal cells in WT mouse prostate (Fig. 2A), the loss of *Abcg2* may have a direct influence on the non-luminal cells. To understand the significance of *Abcg2* loss in the non-luminal cells, the number of p63 expressing basal cells was quantified per prostate gland. No difference was observed in the number of p63 expressing basal cells per prostate gland in the Abcg2 null ventral prostates after one and five cycles of regression and regeneration (Fig. 2B). The sphere formation efficiency determines in vitro proliferation and differentiation potential of basal and stem/progenitor cells [31]. Although the number of p63 expressing basal cells was not changed after one and five cycles of regression and regeneration (Fig. 2B), a significant increase in the sphere formation efficiency was observed in Abcg2 null ventral prostate cells compared with WT prostate cells in the intact group ($P < 0.01$) (Fig. 2C). Moreover, the increase in sphere formation efficiency was more profound in Abcg2 null prostate cells compared with WT prostate cells after one cycle of regression and regeneration ($P < 0.05$) (Fig. 2C). Sphere formation efficiency was tested after five cycles of regression and regeneration in one experiment. Results from one representative experiment (circled in Fig. 2C) from intact and one cycle of Cx + T groups were compared with results from five cycles of Cx + T group (Fig. 2D). Regenerated Abcg2 null ventral prostates after five cycles of Cx + T showed approximately eightfold increase in sphere number/well compared with regenerated WT ventral prostates ($P < 0.001$) (Fig. 2D). The sphere formation efficiency decreased approximately fivefold ($P < 0.001$) in WT and approximately twofold ($P < 0.001$) in Abcg2 null prostate cells after five cycles of regression and regeneration compared with one cycle of regression and regeneration. The decrease in sphere formation efficiency after five cycles of regression and regeneration suggests exhaustion of stem/progenitor cell pool after repeated prostate regression and regeneration. The decrease in sphere formation efficiency after five cycles of regression and regeneration in WT prostate cells was more pronounced than in Abcg2 null prostate cells. This suggests that enhanced activation of stem/progenitor cell pool in Abcg2 null prostate was not accompanied with profound stem cell exhaustion until the fifth cycle of Cx + T in Abcg2 null prostate.

Since *Abcg2* loss resulted in enhanced sphere formation efficiency, we speculated that pharmacological inhibition of ABCG2 in WT prostate cells may lead to enhanced sphere formation efficiency. However, pharmacological inhibition of ABCG2 with Ko143 resulted in significantly decreased number of spheres derived from WT ventral prostate cells (Fig. 2E). A decrease in sphere number after Ko143 treatment in WT prostate cells suggests that enhanced sphere formation efficiency in Abcg2 null prostate cells was due to systemic effects of *Abcg2* deletion.

We speculated that highly enhanced sphere formation efficiency after prostate regression and regeneration was a result of enhanced stem/progenitor cell activation in Abcg2 null ventral prostates compared with WT controls. Enhanced stem/progenitor cell activation may lead to exhaustion of self-renewal and differentiation ability after repeated regression and regeneration cycles, leading to impairment of prostate regeneration. Hence, we hypothesized that prostate regeneration may be impaired after repeated regression and regeneration cycles. To assess differences in the regenerative ability between Abcg2 null and WT mouse prostates; ventral prostate weights were measured. Regenerated prostates from both WT and Abcg2 null mice showed reduced weights compared with intact prostates, because exogenous testosterone was given for 1 week. Prostate regeneration to the original intact size requires 2–3 weeks of testosterone treatment. After one cycle of regression and regeneration, the ventral prostate weights did not differ in Abcg2 null mice compared with WT mice (Fig. 2F). However, after five cycles of regression and regeneration, the ventral prostate weights decreased in Abcg2 null mice compared with WT mice, but change was not statistically significant (Fig. 2F). Non-significant difference in ventral prostate weights suggests that regeneration ability of Abcg2 null prostate cells was unaffected after five cycles of androgen deprivation and replacement. Hence, enhanced stem/progenitor cell activation after repeated regression and regeneration in Abcg2 null prostates was not accompanied with stem/progenitor cell exhaustion and prostate regeneration impairment.

Abcg2 null prostates undergo more differentiating divisions in sphere culture

Since sphere formation efficiency was significantly higher in Abcg2 null prostate cells compared with WT prostate cells, the ability of sphere-forming cells to proliferate and differentiate was analyzed further. Moreover, basal and basal stem/progenitor specific role of Abcg2 was studied in the sphere formation assay. To determine the proliferation and differentiation characteristics of Abcg2 null prostate cells, spheres were characterized in terms of size, lumen formation, labeling of proliferating cells, and expression of differentiation markers. Abcg2 null prostate cells generated larger spheres compared with WT controls at day 7 ($P < 0.01$) and day 14 ($P = 0.06$), suggesting increased proliferation and/or differentiation (Fig. 3A). Heterogeneity in sphere sizes was observed at day 14 of sphere culture. Spheres were counted by categorizing them as small ($< 250\ \mu m$) and large ($> 250\ \mu m$). The numbers of both small and large spheres were significantly increased in Abcg2 null prostate cells compared with WT prostate cells ($< 250\ \mu m$, $P < 0.001$; $> 250\ \mu m$, $P < 0.01$) (Fig. 3B). Sizes of the small spheres did not change; sizes of the large spheres were significantly increased in Abcg2 null prostate cells compared with WT prostate cells ($P < 0.01$)

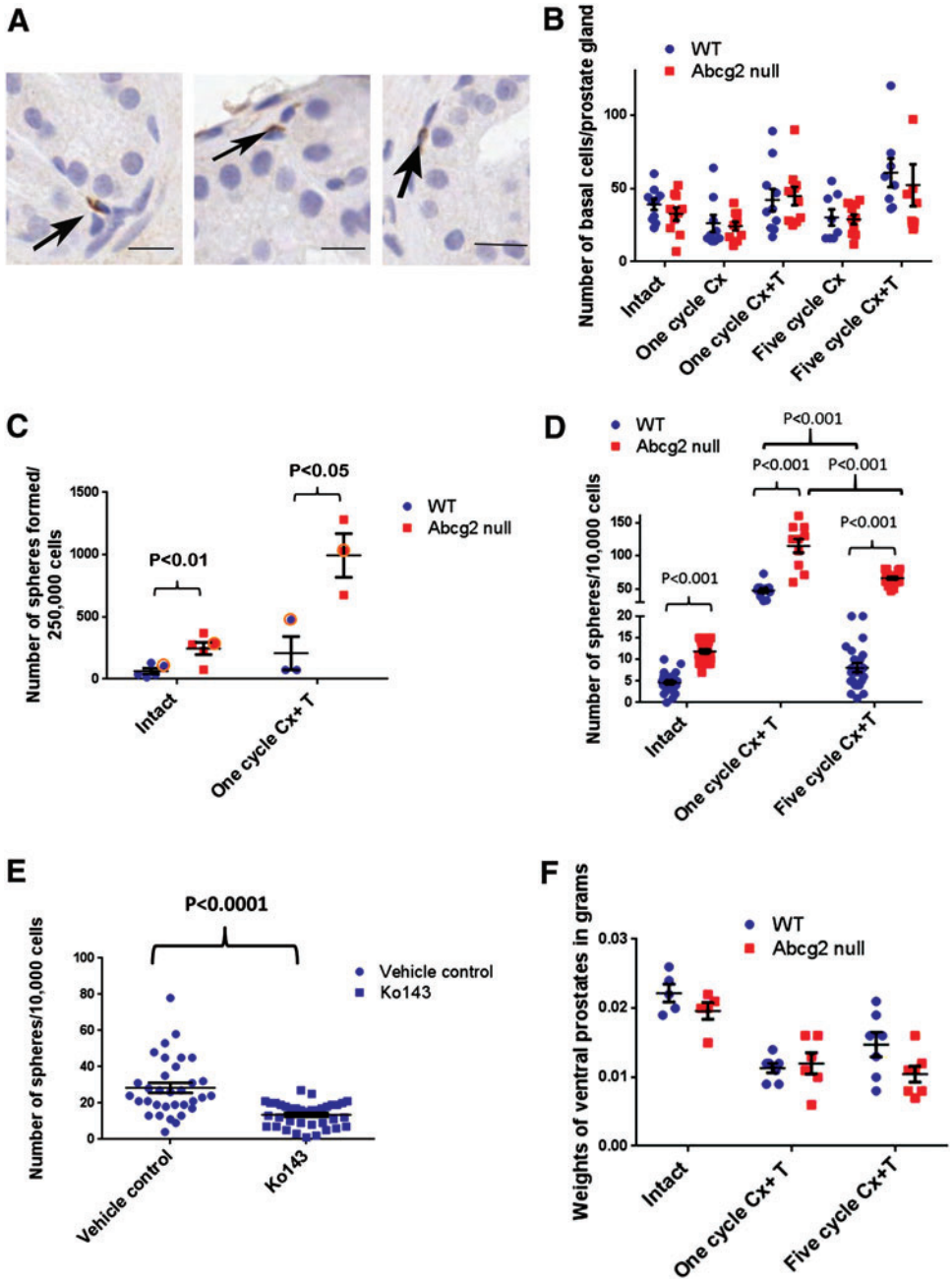

FIG. 2. Sphere formation efficiency is augmented in Abcg2 null mouse prostate. **(A)** Immunohistochemistry staining using antibody against Abcg2 showing rare Abcg2 expressing cells (*arrows*) in non-luminal cells, bar = 20 μm. **(B)** Quantitation of $p63^+$ immunostained basal cells in WT ($n = 3$) and Abcg2 null ($n = 3$) ventral prostate sections. Quantitation was performed on images captured from 10 representative prostate ducts; 3 ducts from each mouse. (Intact, $P = 0.26$; one cycle Cx, $P = 0.77$, one cycle Cx + T, $P = 0.80$; 5 cycle Cx, $P = 0.83$; five cycles Cx + T, $P = 0.64$; calculated using Student's *t* tests) **(C)** Quantitation of number of spheres formed/2.5×10^5 cells plated ($n = 5$ experiments; each experiment was performed by combining four ventral prostates; intact, $P < 0.01$, one cycle Cx + T, $P < 0.05$, calculated using Student's *t* test). **(D)** One representative experiment (*circled*) from **(C)** showing sphere formation efficiency in intact ($n = 24$ wells) and one cycle of Cx + T ($n = 10$ wells) ($P < 0.001$, calculated using Student's *t* test). Quantitation of number of spheres/well from one independent experiment after five cycles of Cx + T, ($n = 24$ wells) ($P < 0.001$, calculated using Student's *t* test). Comparison between spheres derived from prostate cells from both the genotypes after five cycles of regression and regeneration compared with one cycle of regression and regeneration was significantly different using ANOVA ($P < 0.001$, calculated using Student's *t* test). **(E)** Sphere formation efficiency of WT prostate cells after pharmacological inhibition of ABCG2 with Ko143, ($n = 30$ wells) ($P < 0.001$, calculated using Student's *t* test). **(F)** Ventral prostate weights in grams after five cycles of regression (Cx) and regeneration (+T) for intact ($n = 5$), one cycle ($n = 6$), 5 cycles ($n = 7$) (Intact, $P = 0.17$; one cycle Cx + T, $P = 0.66$; five cycle Cx + T, $P = 0.066$; calculated using Student's *t* test). Color images available online at www.liebertpub.com/scd

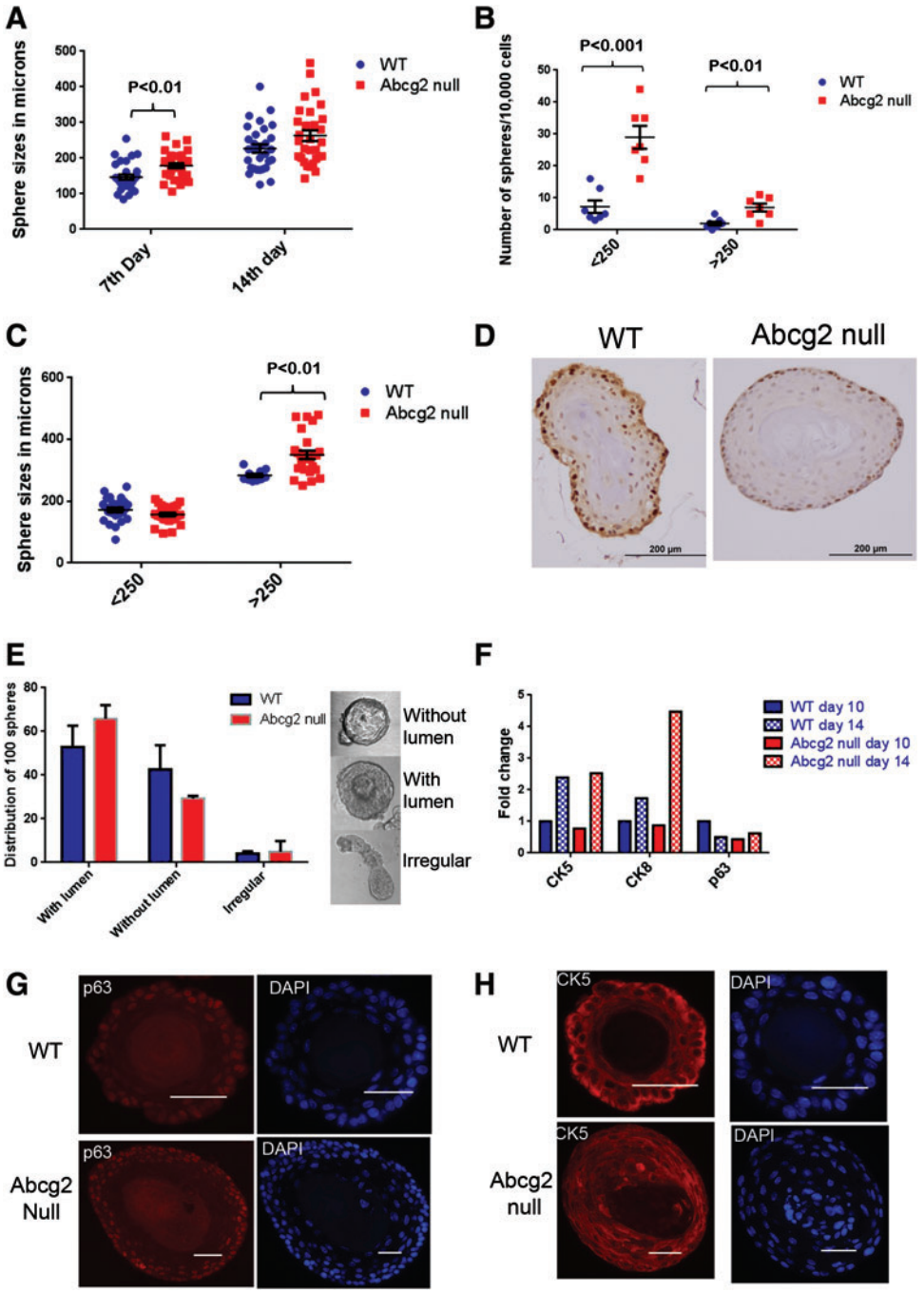

FIG. 3. Sphere formation efficiency is increased with enhanced differentiation in Abcg2 null prostate cells. **(A)** Sphere sizes in microns. Spheres generated from Abcg2 null prostate cells were compared with WT controls after 7 ($n=30$) and 14 days ($n=30$) of sphere culture. Size measurements of spheres from two separate experiments were combined (7th day, $P<0.01$; 14th day, $P=0.06$; calculated using Student's t test). **(B)** Sphere counts in two different categories: small ($<250\,\mu m$) and large ($>250\,\mu m$) ($n=7$) ($<250\,\mu m$, $P<0.001$; $>250\,\mu m$, $P<0.01$ calculated using Student's t tests). **(C)** Sizes of spheres from two different categories: small ($<250\,\mu m$) and large ($>250\,\mu m$) (large spheres, $P<0.01$, calculated using Student's t tests). **(D)** Immunohistochemistry staining using antibody against Ki67 proliferation marker, showing Ki67 expressing brown cells in large spheres generated from WT and Abcg2 null prostate cells on day 14 of sphere culture. **(E)** Distribution of 100 spheres categorized as with lumen, without lumen, and irregular ($n=3$ experiments; with lumen, $P=0.4$; without lumen, $P=0.4$; irregular, $P=0.8$, calculated using Student's t tests). **(F)** RNA quantitation of cytokeratin 5 (CK5), CK8, and p63 from spheres derived from WT and Abcg2 null prostate cells on 10th and 14th day of sphere culture. Each quantitative reverse transcription-PCR (qRT-PCR) was performed in triplicate. Each sample was normalized to endogenous GAPDH mRNA, and fold changes were calculated by normalizing each sample to mRNA expression of genes in spheres derived from WT prostate cells at day 10. **(G)** Immunofluorescence staining of spheres generated from WT and Abcg2 null prostate cells using antibody against p63 and with DAPI stained nuclei. Scale bars = 50 µm. **(H)** Immunofluorescence staining of spheres generated from WT and Abcg2 null prostate cells using antibody against CK5 and with DAPI-stained nuclei. Scale bars = 50 µm. Color images available online at www.liebertpub.com/scd

(Fig. 3C). Hence, we speculated that proliferation was increased in the large spheres derived from Abcg2 null prostate cells compared with WT spheres having a similar perimeter. Hence, the labeling of proliferating cells in the large spheres was assessed using expression of Ki67 proliferation marker in immunohistochemistry. The large spheres derived from Abcg2 null prostate cells showed presence of proliferating cells only at the outer edges similar to large spheres derived from WT prostate cells (Fig. 3D). The apoptosis marker Caspase3 was not expressed in spheres derived from either WT or Abcg2 null prostate cells, suggesting no change in apoptosis rate (data not shown). At the time of labeling, the majority of cells may have already undergone multiple differentiating divisions, resulting in no detectable difference in the proliferation pattern of large spheres derived from Abcg2 null prostate cells compared with WT spheres having a similar perimeter.

Since spheres derived from Abcg2 null prostate cells did not display an increase in proliferative cells, progression of differentiation in sphere culture was examined. Lumen formation in sphere cultures indicates enhanced differentiation of epithelial cells [36]. At day 7 of sphere culture, a fraction of spheres show lumen formation while the other fraction shows solid structure without lumen formation (Fig. 3E). At day 14, all the spheres showed lumen formation and were not included in these studies. Hence, the spheres on day 7 were categorized as with lumen, without lumen, and irregular (Fig. 3E). The differences between spheres from different categories derived from WT and Abcg2 null ventral prostate cells were not significant (Fig. 3E). These data indicate that lumen formation in sphere culture was not affected due to the loss of *Abcg2*. To understand the progression of differentiation further, quantitation of mRNA for lineage markers was performed at day 10 and 14 of sphere culture. Quantitation of p63 mRNA expression demonstrated a twofold reduction in Abcg2 null spheres at day 10 compared with WT controls without profound changes in CK5 and CK8 expression (Fig. 3F). A decrease in p63 mRNA at an earlier time point compared with WT controls suggests enhanced differentiation toward $p63^-$ cells. Moreover, at day 14, expression of CK5 and CK8 increased in both spheres derived from WT and Abcg2 null prostate cells (Fig. 3F). The increase in CK8 expression at sphere culture day 14 was $\sim$4.5-fold in spheres derived from Abcg2 null prostate cells compared with WT controls. Thus, the data indicate that the Abcg2 null prostate cells undergo more differentiating divisions toward $p63^-$ and CK8 expressing cells.

Previous studies demonstrate that deletion of genes critical for prostate epithelial differentiation, for example *Lgr4*, resulted in differentiation failure toward $p63^-$ cells in sphere culture [37]. Hence, immunofluorescence staining was performed to determine whether spheres derived from Abcg2 null prostate cells show aberrant differentiation at day 14 of sphere culture. Spheres derived from WT and Abcg2 null prostate cells were analyzed using immunofluorescence staining for different lineage markers, for example, p63, CK5, and CK8. Localization of CK5 and p63 did not show detectable differences in the spheres derived from Abcg2 null prostate cells compared with WT controls (Fig. 3G, H). Expression of p63 was detected in the cells at the outer edges of spheres derived from Abcg2 null prostate cells similar to WT controls (Fig. 3G). CK8 expression was not observed in WT and Abcg2 null spheres at day 14 using immunofluorescence staining. Previous studies document inability to detect high CK8 protein expression in spheres before day 14 [31]. Dual immunofluorescence staining of p63 and CK5 showed heterogeneity in terms of colocalization of p63 and CK5. The majority of spheres derived from WT and Abcg2 null cells showed expression of p63 in a small fraction of cells, while CK5 expression was observed in a large fraction of cells (Supplementary Fig. S2). A fraction of spheres derived from Abcg2 null prostate cells showed very rare $p63^+$ cells (Supplementary Fig. S2E–H), while the other fraction showed a higher number of $p63^+$ cells (Supplementary Fig. S2I–J). The heterogeneity in colocalization of p63 and CK5 was higher in spheres derived from Abcg2 null prostate cells (Supplementary Fig. S2E–J) than WT controls (Supplementary Fig. S2A–D) mainly due to higher variability in the sizes and morphologies of spheres.

Thus, the data indicate that the sphere formation efficiency was increased in the Abcg2 null prostate cells with higher variability in sizes compared with WT prostate cells, with no aberrant differentiation pattern. However, the pooled spheres derived from Abcg2 null prostate cells showed increased mRNA expression of CK8 and decreased p63 mRNA expression, suggesting enhanced number of differentiating divisions.

Decreased sphere formation efficiency and enhanced differentiation when MDR-ABC transporters are inhibited

Since the absence of *Abcg2* expression resulted in more differentiating divisions, we speculated that inhibition of ABCB1 and ABCC1 transporters results in enhanced differentiation. First, the mRNA levels of *Abcb1a/b* and *Abcc1* were determined in WT and Abcg2 null prostate Lin^- Sca^{high} $CD44^{high}$ cells using qRT-PCR. *Abcb1a/b* and *Abcc1*mRNA levels did not show a difference between Abcg2 null Lin^-Sca^{high} $CD44^{high}$ cells and WT controls (data not shown). Next, to determine the efflux function of ABCB1 and ABCC1 transporters in WT ventral prostate cells, Hoechst efflux was determined using the side population assay. Concomitant staining of cells with fluorescent-conjugated antibodies against lineage markers was performed to distinguish between the lineage-positive (Lin^+) and lineage-negative (Lin^-) side population. In the Lin^- population, 0.5%–0.7% cells had the side population phenotype (Lin^- side population). In contrast, 1.1%–5.2% of the Lin^+ cells had the side population phenotype (Lin^+ side population) (Fig. 4A). The Lin^- side population of WT prostate cells contained cells expressing high levels of prostate basal stem/progenitor markers Sca (56.4%) and CD44 (35.1%), confirming the efflux ability in the basal stem/progenitor cells (Fig. 4B). To confirm the requirement of MDR-ABC transporters in Hoechst efflux, inhibition of ABCB1 and ABCC1 transporters was performed using 1 μM reversan in WT prostate cells. Reversan at the concentration used completely eliminated the Lin^- side population of WT ventral prostate (Fig. 4C), suggesting a critical role of MDR-ABC transporters in maintaining the side population phenotype. At the concentration used, reversan inhibited all of

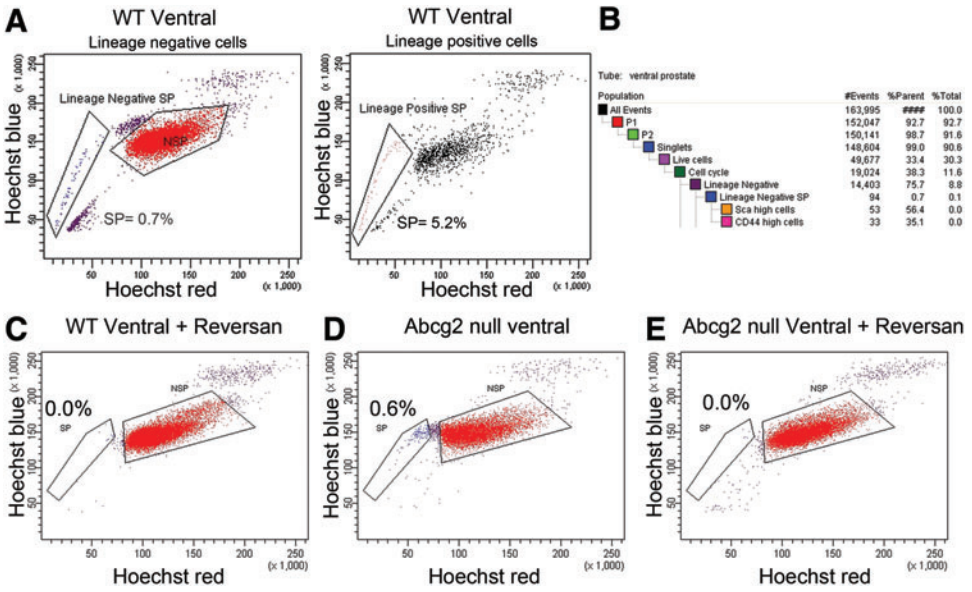

FIG. 4. Presence of side population in WT and Abcg2 null prostate cells. **(A)** Lin^- side population of WT ventral prostate is 0.7% of total Lin^- cells, while Lin^+ side population is 5.2% of total Lin^- cells in a representative experiment. Experiment was performed thrice. **(B)** Population hierarchy statistics generated by BDFACS Diva software showing Sca^{high} (56.4%) and $CD44^{high}$ (35.1%) cells in Lin^- side population from WT ventral prostate. **(C)** Elimination of Lin^- side population from WT ventral prostate with 1 μM reversan treatment. **(D)** Lin^- side population in Abcg2 null ventral prostate cells. **(E)** Elimination of Abcg2 null Lin^- side population with 1 μM reversan treatment. Color images available online at www.liebertpub.com/scd

the MDR-ABC efflux transporters, including ABCG2. Next, to determine the efflux function of ABCB1 and ABCC1 transporters in Abcg2 null ventral prostate cells, the side population assay was performed. The Lin^- side population was detected in Abcg2 null prostate cells (Fig. 4D) and was completely eliminated using 1 μM reversan (Fig. 4E). The presence of ABCB1 and ABCC1 efflux function in the Abcg2 null prostate basal stem/progenitor cells (Fig. 4D) indicates that inhibition of ABCB1 and ABCC1 may modulate basal and basal stem/progenitor cell function.

Sphere formation efficiency examines proliferation and differentiation of basal and basal stem/progenitor cells. We hypothesized that inhibition of MDR-ABC efflux may modulate sphere formation efficiency. To test the hypothesis, inhibition of MDR-ABC transporters was performed using 1 and 5 μM reversan in WT and Abcg2 null prostate cells in the sphere formation assay. Sphere number and expression of differentiation markers p63, CK5, and CK8 were used to analyze proliferation and differentiation of WT and Abcg2 null prostate cells. The number of spheres derived from WT prostate cells significantly decreased with 5 μM reversan treatment ($P < 0.01$) but not when treated with 1 μM reversan (Fig. 5A). Sphere formation efficiency in Abcg2 null prostate cells significantly decreased in the presence of 1 and 5 μM reversan ($P < 0.001$) (Fig. 5A). CK5, CK8, and p63 differentiation marker expression was examined in spheres with reversan treatment using qRT-PCR. Spheres derived from WT prostate cells did not show alteration in CK5 and CK8 expression profile, and p63 expression increased with 1 μM reversan treatment (Fig. 5B). However, spheres derived from WT prostate cells demonstrated increased CK5 and CK8 expression after 5 μM reversan treatment (Fig. 5B). Spheres derived from Abcg2 null prostate cells demonstrated increased CK5 and CK8 expression with both 1 and 5 μM reversan compared with vehicle control, suggesting differentiation from basal stem/progenitor to luminal phenotype (Fig. 5B). Expression of p63 did not change after 1 and 5 μM reversan treatments in spheres derived from Abcg2 null prostate cells (Fig. 5B).

Since spheres derived from Abcg2 null prostate cells showed enhanced differentiation after 14 days and reversan treatment augmented the differentiation further, we hypothesized that ABCG2 inhibition in WT prostate cells enhances differentiation. We inhibited MDR-ABC transporters with Ko143 and reversan to determine the WT prostate cell differentiation pattern. Spheres derived from WT prostate cells showed increased CK8 expression with Ko143 treatment. However, reversan treatment caused the highest augmentation in CK8 expression and differentiation toward luminal phenotype (Fig. 5C). Since reversan treatment caused maximum differentiation in sphere culture, the consequence of MDR-ABC efflux inhibition was determined using reversan during prostate regeneration. We hypothesized that Abcg2 null mouse prostates are more sensitive to MDR-ABC efflux inhibition compared with WT mouse prostates, because embryonic deletion of *Abcg2* may render Abcg2 null mouse prostates more dependent on ABCB1/C1. MDR-ABC efflux transporters were pharmacologically inhibited using reversan during prostate regeneration after androgen deprivation cycle in WT and Abcg2 null mice (Fig. 5D). Ventral prostate luminal and basal cells were counted in WT and Abcg2 null mouse prostate duct cross-sections. The least convoluted ducts were selected from the proximal prostate (Supplementary Fig. S1). Basal and luminal cells were quantitated in reversan-treated WT prostates to reversan-treated Abcg2 null prostates to

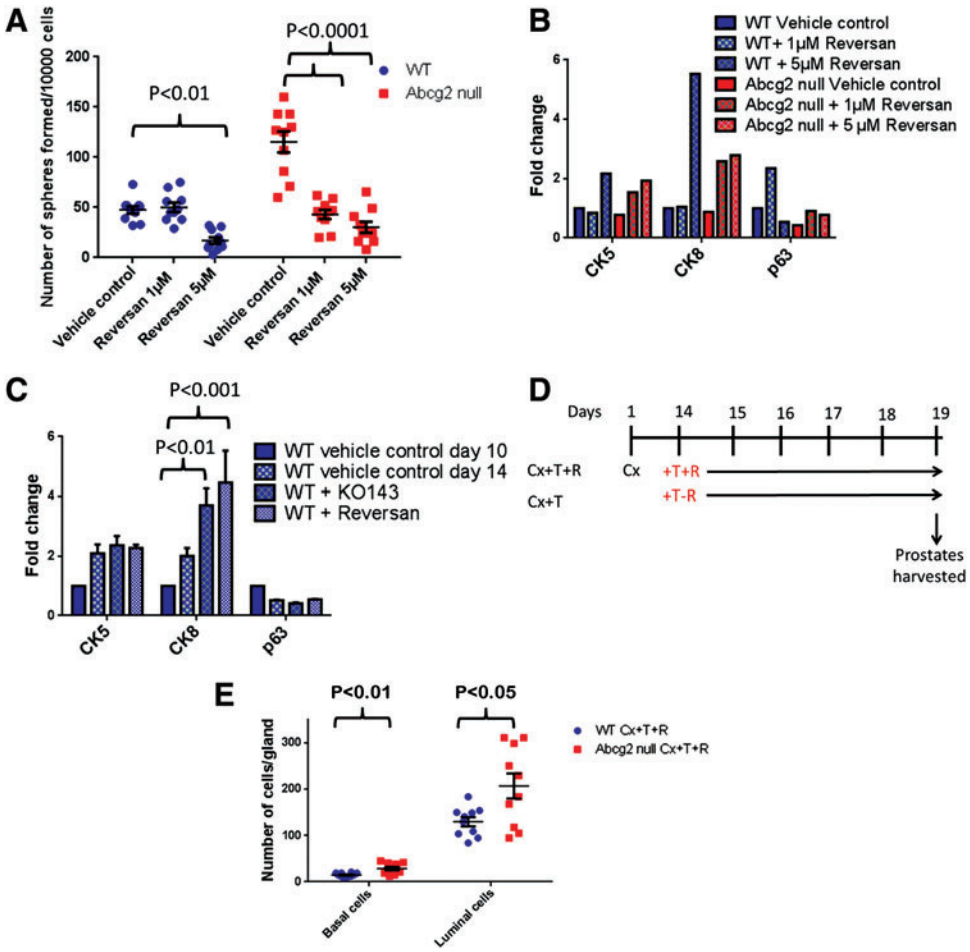

FIG. 5. Multi-drug resistance-ATP binding cassette (MDR-ABC) efflux inhibition causes decreased sphere formation efficiency and enhanced differentiation. **(A)** Number of spheres/well ($n=12$) from a representative experiment showing statistically significant decrease in spheres generated from WT prostate cells and Abcg2 null prostate cells when treated with 1 and 5 μM reversan (*P* values were calculated using two way ANOVA). **(B)** Fold changes in mRNA levels quantitated using qRT-PCR with and without reversan treatment. Each qRT-PCR was performed in triplicate. Each sample was normalized to endogenous GAPDH mRNA, and fold change was calculated by normalizing each sample to mRNA expression of genes in spheres derived from WT prostate cells at day 10. **(C)** Fold changes in mRNA levels quantitated using qRT-PCR with KO143 and reversan treatment ($n=2$ experiments). Each qRT-PCR was performed in triplicate for each experiment. Each sample was normalized to endogenous GAPDH mRNA, and fold changes were calculated by normalizing each sample to mRNA expression of genes in spheres derived from WT prostate cells at day 10 (*P* values were calculated using two way ANOVA). **(D)** Schematic representation of reversan treatment experimental strategy during prostate regeneration. **(E)** Quantitation of $p63^+$ basal cells and $p63^-$ luminal cells in WT Cx + T + R ($n=3$) and Abcg2 null Cx + T + R ($n=3$) ventral prostate sections immunostained for p63. Quantitation was performed on images captured from 10 representative prostate ducts; 3–4 ducts from each mouse (*P* values calculated using Student's *t* test). Color images available online at www.liebertpub.com/scd

determine whether Abcg2 null mouse prostates are more sensitive to ABCB1/C1 inhibition compared with WT mouse prostates. Reversan-treated Abcg2 null mice showed a statistically significant increase in basal as well as in luminal cell numbers/prostate gland compared with reversan-treated WT mice (Fig. 5E).

Thus, inhibition of MDR-ABC efflux decreased sphere formation efficiency, indicating a decrease in stem/progenitor cell activation. Moreover, increased expression of CK5 and CK8 suggests enhanced epithelial differentiation, with inhibition of MDR-ABC efflux in sphere culture. In addition, Abcg2 null mouse prostates showed an increased number of basal and luminal cells compared with WT mouse prostates, with inhibition of MDR-ABC efflux during regeneration. Increased number of basal and luminal cells suggests enhanced prostate epithelial differentiation with inhibition of MDR-ABC efflux.

Discussion

We used the Abcg2 null mouse model and MDR-ABC transporter inhibition to understand the consequence of inhibiting ABCB1, ABCC1, and ABCG2 transporter activity on prostate epithelial differentiation of the murine prostate. In the Abcg2 null mouse model, *Abcg2* is deleted embryonically; hence, the role of Abcg2 in the prostate basal and

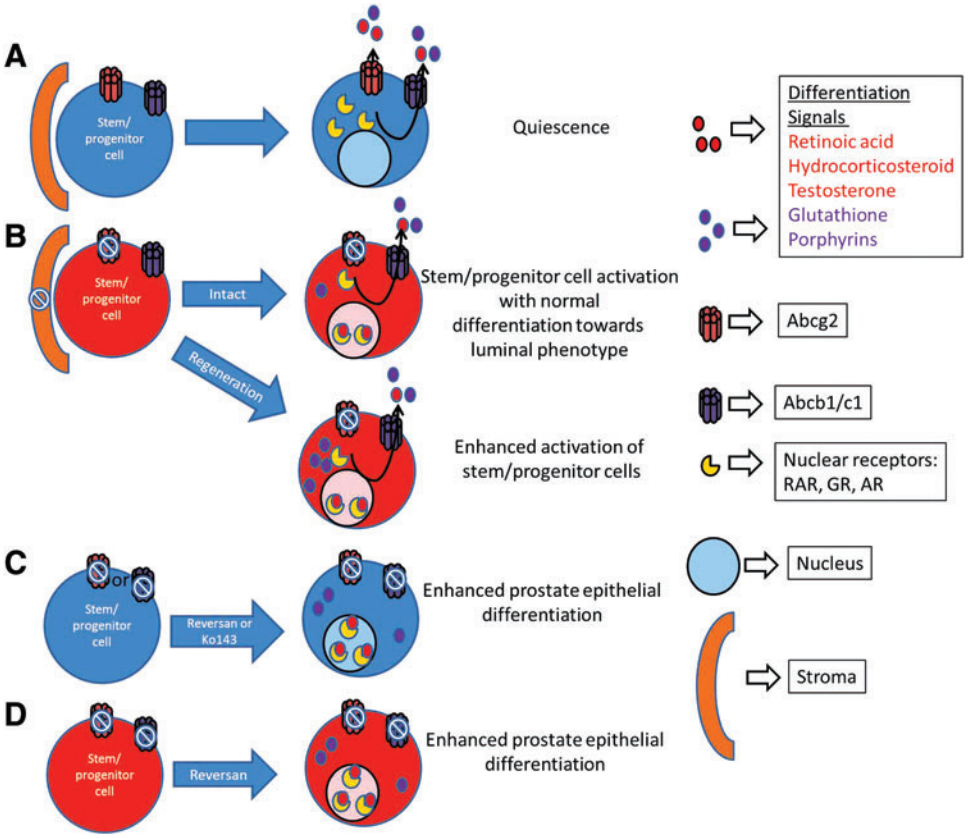

FIG. 6. Model of enhanced differentiation through MDR-ABC efflux transporter inhibition. **(A)** Cells with active MDR-ABC efflux transporters are quiescent and have undetectable steroid receptors and differentiation signals. **(B)** Systemic Abcg2 deletion/inhibition in stroma and epithelia leads to activation of stem/progenitor cell niche and normal differentiation toward luminal phenotype. Moreover, after prostate regression and regeneration cycles, Abcg2 deletion leads to enhanced activation of stem/progenitor cells. Enhanced activation of stem/progenitor niche may be due to oxidative stress induced by androgen deprivation and the highest accumulation of glutathione and porphyrins. **(C)** Complete MDR-ABC efflux inhibition in WT prostate cells with either reversan or Ko143 leads to enhanced prostate epithelial differentiation, possibly due to an increased accumulation of differentiation signals (eg, retinoic acid, hydrocorticosteroid, testosterone, glutathione, and porphyrins). Activation of steroid receptor signaling and alteration in the redox status may lead to enhanced differentiation. **(D)** Complete MDR-ABC efflux inhibition in ABCG2 null prostate cells with reversan leads to enhanced prostate epithelial differentiation, possibly due to an increased accumulation of differentiation signals (eg, retinoic acid, hydrocorticosteroid, testosterone, glutathione, and porphyrins). Color images available online at www.liebertpub.com/scd

luminal cell compartments could be due to systemic effects. Prostate-specific and/or inducible *Abcg2* deletion would allow examination of Abcg2 function without systemic effects.

The role of Abcg2 in the overall prostate structure is compensated by Abcb1 and Abcc1

Abcg2 expression is not required for prostate development, as the presence of compensatory transporters resulted in no profound difference in the Abcg2 null mouse prostate structure. In this study, we demonstrated the presence of the side population phenotype in the Abcg2 null ventral prostate, supporting the existence of ABCB1 and ABCC1 efflux function. In the single transporter knockout mouse models, compensatory effects for the knocked out transporter are common, since ABCB1, ABCC1, and ABCG2 demonstrate similar substrate specificity [38]. There is a variation in the requirement of specific MDR-ABC transporter to maintain the side population phenotype in different tissues. For example, compensatory effects of other transporters do not appear in Abcg2 null hematopoietic stem cells, since the side population phenotype and regeneration ability was not compensated [29]. On the other hand, in Abcg2 null mammary tissue, the side population and the ABCB1 and ABCC1 functional activity increased, suggesting Abcg2 functional compensation by other MDR-ABC efflux pumps [39]. The discrepancy in the requirement of different MDR-ABC transporters to maintain the side population phenotype in different tissues suggests tissue-specific variation in the MDR-ABC transporter expression. Studying prostate differentiation in *Abcb1*, *Abcc1*, *Abcg2* triple, or inducible knockout mice might shed light on the MDR-ABC efflux function without compensatory effects.

Abcg2 loss activates prostate stem/progenitor cell niche, leading to increased sphere formation efficiency

In this study, Abcg2 null prostate cells generate more spheres compared with the WT prostate cells. Increased

sphere formation efficiency may be a collective effect of stem/progenitor cell activation in the basal cell compartment and reduction in the luminal cell number. After prostate regression and regeneration the increase in the sphere formation efficiency was heightened. During androgen-induced prostate regeneration, basal and luminal cell proliferation occurs similar to the normal cell proliferation pattern observed in the prostate [40]. Hence, enhanced sphere formation efficiency in Abcg2 null prostate cells reveals an alteration in the stem/progenitor cell homeostasis. Enhanced stem/progenitor cell activation in Abcg2 null prostate is due to systemic effects of *Abcg2* loss, since in vitro pharmacological inhibition of ABCG2 with Ko143 decreased the number of spheres. Due to the systemic effects of *Abcg2* loss, we cannot pinpoint the exact mechanism for stem/progenitor cell activation. We propose two different possibilities for stem/progenitor cell activation:

First, stem/progenitor cell activation in Abcg2 null mouse prostate may be a result of altered tissue microenvironment and stem cell niche. Abcg2 is highly expressed in the WT mouse prostate vasculature (Supplementary Fig. S3A), and the Lin^+ side population is reduced in Abcg2 null mouse prostate compared with WT prostate (Supplementary Fig. S3B, C). Since stem cell niche in prostate is highly vascularized [41], Abcg2 expression in vasculature may play a critical role in the prostate stem cell niche.

Second, Abcg2 loss may lead to increased intracellular accumulation of Abcg2 substrates, porphyrins [42–45] and glutathione [46], in turn, altering the stem cell redox state [47] and leading to activation of the stem cell niche [48,49]. The cellular redox status is crucial to the balance between stem/progenitor self-renewal and differentiation in various tissues [50]. Androgen deprivation causes an increase in reactive oxygen species and oxidative stress in the prostate [51], which may strongly activate stem/progenitor cells in the Abcg2 null prostate. Apart from steroid efflux function, Abcg2 may have a role in maintaining the redox status of prostate stem/progenitor cells.

Abcg2 deletion leads to enhanced differentiation in stem/progenitor cells

Spheres derived from Abcg2 null prostate cells showed enhanced differentiating divisions compared with WT controls. An increased CK8 mRNA expression in the spheres generated by Abcg2 null prostate cells at day 14 compared with WT controls implies enhanced epithelial differentiation. Moreover, pharmacological inhibition of ABCG2 with Ko143 increased differentiation marker signature in spheres derived from WT prostate cells. Luminal marker expression in sphere culture examines the differentiation potential of basal stem/progenitor cells, which may not be the case in vivo. The luminal cell compartment is regenerated from stem/progenitor cells in the luminal cell compartment, though a very small basal cell fraction has plasticity to differentiate into luminal cells during regeneration and in sphere culture [9]. Hence, lineage tracing of Abcg2 expressing cells would shed light on their in vivo differentiation potential during prostate development and regeneration.

Enhanced differentiation with MDR-ABC efflux inhibition may be multifactorial

The key finding of this study is enhanced luminal differentiation when ABCB1, ABCC1, and ABCG2 are inhibited in spheres. We show that without MDR-ABC efflux function, the sphere number decreased in WT and Abcg2 null prostate cells and spheres demonstrated increased epithelial differentiation compared with vehicle-treated controls. The reversan dose required for the sphere number reduction and increased expression of differentiation markers in Abcg2 null prostate cells was lower than the reversan dose required for the same effect in WT prostate cells, indicating sensitization of Abcg2 null prostate cells for the MDR-ABC efflux function requirement. The reduction in the sphere number can be attributed to the loss of cell proliferation in the sphere-forming cells when MDR-ABC efflux transporters are inhibited. The model shown in Fig. 6 summarizes our observations. The exact mechanism of enhanced differentiation is not yet known. Enhanced differentiation may be a result of an alteration in the intracellular accumulation of differentiating agents, for example, retinoic acid and/or hydrocorticosteroid in the PrEGM media. Moreover, glutathione transport modulation by MDR-ABC transporters [46,52,53] may change the cell's redox state, leading to differentiation [47,48]. The two distinct responses of sphere-forming cells to inhibition of MDR-ABC efflux are as follows: (1) Decreased cell proliferation and (2) enhanced differentiation may be due to discrepancy in the expression of MDR-ABC transporters in distinct populations of sphere-forming cells. During regeneration, inhibition of MDR-ABC efflux resulted in an increased number of basal and luminal cells in Abcg2 null mouse prostates compared with WT mouse prostates, suggesting enhanced prostate epithelial differentiation. Enhanced prostate epithelial differentiation in Abcg2 null mouse prostates compared with WT mouse prostates indicates sensitization of Abcg2 null prostate cells for the requirement of MDR-ABC efflux function. In conclusion, deletion of *Abcg2* leads to ex vivo stem/progenitor cell activation and differentiation and further inhibition of *Abcb1* and *Abcc1* leads to enhanced epithelial differentiation (Fig. 6).

MDR-ABC transporters are potential targets for differentiation therapy of prostatic diseases

ABCG2 participates in the steroid hormone efflux, for example, estrogens [54–56], androgens [12]. DHT is an androgen receptor (AR) ligand. When bound to AR, DHT causes stabilization, conformational activation, and AR nuclear localization, leading to target gene activation or repression and causing cell proliferation or differentiation. AR signaling is the major therapeutic target in aggressive prostate cancers and benign prostatic hyperplasia (BPH). However, targeting AR signaling alone leads to drug resistance and disease recurrence. Hence, targeting multiple pathways could be a more effective approach. In advanced prostate cancer, MDR-ABC transporters are highly expressed [57]. Here, we provide a proof of concept, that prostate luminal cell differentiation can be augmented by MDR-ABC transporter blockade. We propose that differentiation therapy [58] through MDR-ABC efflux inhibition

and subsequent androgen retention in stem/progenitor cells may improve the efficacy of androgen deprivation therapy for prostate cancer and BPH.

Acknowledgments

This work was supported by National Institutes of Health (NIH) (R01DK091240) to W.J.H., CA179907 to D.W.G., the NCI Cancer Center Support Grant (CA016056) to RPCI, and C.L.F. was supported by P30CA016056-S. The authors thank Dr. Brian Sorrentino for generously providing Abcg2 null mice; Dr. Pamela Hershberger for assistance in editing this article; the Mouse Tumor Models Resource core facility, especially Bryan Gillard for animal care, Ellen Karasik for assistance with prostate dissections and histological preparations. They also thank the Flow and Image Cytometry core facility, especially Earl Timm and Dr. Craig Jones for their assistance in flow cytometry experiments. They thank the Pathology Resource Network core facility, especially Erika VanDette for scanning the immunohistochemistry slides.

Author Disclosure Statement

The authors have the following conflicts: W.J.H.: RPCI patent holder titled ''Methods for evaluating and implementing prostate disease treatments'' patent no. 8048640.

References

1. Cunha GR, AA Donjacour, PS Cooke, S Mee, RM Bigsby, SJ Higgins and Y Sugimura. (1987). The endocrinology and developmental biology of the prostate. Endocr Rev 8:338–362.
2. Coffey DS, J Shimazaki and HG Williams-Ashman. (1968). Polymerization of deoxyribonucleotides in relation to androgen-induced prostatic growth. Arch Biochem Biophys 124:184–198.
3. Isaacs JT and DS Coffey. (1989). Etiology and disease process of benign prostatic hyperplasia. Prostate Suppl 2:33–50.
4. Bonkhoff H and K Remberger. (1996). Differentiation pathways and histogenetic aspects of normal and abnormal prostatic growth: a stem cell model. Prostate 28:98–106.
5. Bonkhoff H. (1996). Role of the basal cells in premalignant changes of the human prostate: a stem cell concept for the development of prostate cancer. Eur Urol 30:201–205.
6. Blackwood JK, SC Williamson, LC Greaves, L Wilson, AC Rigas, R Sandher, RS Pickard, CN Robson, DM Turnbull, et al. (2011). In situ lineage tracking of human prostatic epithelial stem cell fate reveals a common clonal origin for basal and luminal cells. J Pathol 225:181–188.
7. Choi N, B Zhang, L Zhang, M Ittmann and L Xin. (2012). Adult murine prostate basal and luminal cells are self-sustained lineages that can both serve as targets for prostate cancer initiation. Cancer Cell 21:253–265.
8. Liu J, LE Pascal, S Isharwal, D Metzger, R Ramos Garcia, J Pilch, S Kasper, K Williams, PH Basse, et al. (2011). Regenerated luminal epithelial cells are derived from preexisting luminal epithelial cells in adult mouse prostate. Mol Endocrinol 25:1849–1857.
9. Ousset M, A Van Keymeulen, G Bouvencourt, N Sharma, Y Achouri, BD Simons and C Blanpain. (2012). Multipotent and unipotent progenitors contribute to prostate postnatal development. Nat Cell Biol 14:1131–1138.
10. Wang ZA, A Mitrofanova, SK Bergren, C Abate-Shen, RD Cardiff, A Califano and MM Shen. (2013). Lineage analysis of basal epithelial cells reveals their unexpected plasticity and supports a cell-of-origin model for prostate cancer heterogeneity. Nat Cell Biol 15:274–283.
11. Fedoruk MN, P Gimenez-Bonafe, ES Guns, LD Mayer and CC Nelson. (2004). P-glycoprotein increases the efflux of the androgen dihydrotestosterone and reduces androgen responsive gene activity in prostate tumor cells. Prostate 59:77–90.
12. Huss WJ, DR Gray, NM Greenberg, JL Mohler and GJ Smith. (2005). Breast cancer resistance protein-mediated efflux of androgen in putative benign and malignant prostate stem cells. Cancer Res 65:6640–6650.
13. Vander Griend DJ, WL Karthaus, S Dalrymple, A Meeker, AM DeMarzo and JT Isaacs. (2008). The role of CD133 in normal human prostate stem cells and malignant cancer-initiating cells. Cancer Res 68:9703–9711.
14. Pascal LE, AJ Oudes, TW Petersen, YA Goo, LS Walashek, LD True and AY Liu. (2007). Molecular and cellular characterization of ABCG2 in the prostate. BMC Urol 7:6.
15. Foster BA, KJ Gangavarapu, G Mathew, G Azabdaftari, CD Morrison, A Miller and WJ Huss. (2013). Human prostate side population cells demonstrate stem cell properties in recombination with urogenital sinus mesenchyme. PLoS One 8:e55062.
16. Zhou S, Y Zong, T Lu and BP Sorrentino. (2003). Hematopoietic cells from mice that are deficient in both Bcrp1/Abcg2 and Mdr1a/1b develop normally but are sensitized to mitoxantrone. Biotechniques 35:1248–1252.
17. Doyle MJ, S Zhou, KK Tanaka, A Pisconti, NH Farina, BP Sorrentino and BB Olwin. (2011). Abcg2 labels multiple cell types in skeletal muscle and participates in muscle regeneration. J Cell Biol 195:147–163.
18. Higashikuni Y, J Sainz, K Nakamura, M Takaoka, S Enomoto, H Iwata, M Sahara, K Tanaka, N Koibuchi, et al. (2010). The ATP-binding cassette transporter BCRP1/ABCG2 plays a pivotal role in cardiac repair after myocardial infarction via modulation of microvascular endothelial cell survival and function. Arterioscler Thromb Vasc Biol 30:2128–2135.
19. Bunting KD, J Galipeau, D Topham, E Benaim and BP Sorrentino. (1998). Transduction of murine bone marrow cells with an MDR1 vector enables ex vivo stem cell expansion, but these expanded grafts cause a myeloproliferative syndrome in transplanted mice. Blood 92:2269–2279.
20. Ahmed F, N Arseni, H Glimm, W Hiddemann, C Buske and M Feuring-Buske. (2008). Constitutive expression of the ATP-binding cassette transporter ABCG2 enhances the growth potential of early human hematopoietic progenitors. Stem Cells (Dayton, Ohio) 26:810–818.
21. Porro A, N Iraci, S Soverini, D Diolaiti, S Gherardi, C Terragna, S Durante, E Valli, T Kalebic, et al. (2011). c-MYC oncoprotein dictates transcriptional profiles of ATP-binding cassette transporter genes in chronic myelogenous leukemia CD34+ hematopoietic progenitor cells. Mol Cancer Res 9:1054–1066.
22. Burkhart CA, F Watt, J Murray, M Pajic, A Prokvolit, C Xue, C Flemming, J Smith, A Purmal, et al. (2009). Small-molecule multidrug resistance-associated protein 1 inhibitor reversan increases the therapeutic index of chemotherapy in mouse models of neuroblastoma. Cancer Res 69:6573–6580.

23. Chubb C. (1989). Genetically defined mouse models of male infertility. J Androl 10:77–88.
24. Huttunen E, T Romppanen and HJ Helminen. (1982). Testosterone action on the ventral prostate lobe of the castrated rat as assessed with a stereologic morphometric method. Am J Anat 165:199–209.
25. Johnsonbaugh RE, FG Dalldorf, FS French and SN Nayfeh. (1976). Androgen action in the rat ventral prostate: effect of castration and testosterone treatment on polyribosomes. J Steroid Biochem 7:73–79.
26. Belham JE and GE Neal. (1971). Testosterone action in the rat ventral prostate. The effects of diethylstilboestrol and cyproterone acetate on the metabolism of (3 H)testosterone and the retention of labelled metabolites by rat ventral prostate in vivo and in vitro. Biochem J 125:81–91.
27. Banerjee PP, S Banerjee, KI Tilly, JL Tilly, TR Brown and BR Zirkin. (1995). Lobe-specific apoptotic cell death in rat prostate after androgen ablation by castration. Endocrinology 136:4368–4376.
28. Ding XW, JH Wu and CP Jiang. (2010). ABCG2: a potential marker of stem cells and novel target in stem cell and cancer therapy. Life Sci 86:631–637.
29. Zhou S, JJ Morris, Y Barnes, L Lan, JD Schuetz and BP Sorrentino. (2002). Bcrp1 gene expression is required for normal numbers of side population stem cells in mice, and confers relative protection to mitoxantrone in hematopoietic cells in vivo. Proc Natl Acad Sci U S A 99:12339–12344.
30. Kato M, K Ishii, Y Iwamoto, T Sasaki, H Kanda, Y Yamada, K Arima, T Shiraishi and Y Sugimura. (2013). Activation of FGF2-FGFR signaling in the castrated mouse prostate stimulates the proliferation of basal epithelial cells. Biol Reprod 89:81.
31. Lukacs RU, AS Goldstein, DA Lawson, D Cheng and ON Witte. (2010). Isolation, cultivation and characterization of adult murine prostate stem cells. Nat Protoc 5:702–713.
32. Ergen AV, M Jeong, KK Lin, GA Challen and MA Goodell. (2013). Isolation and characterization of mouse side population cells. Methods Mol Biol 946:151–162.
33. Goodell MA, S McKinney-Freeman and FD Camargo. (2005). Isolation and characterization of side population cells. Methods Mol Biol (Clifton, N.J 290:343–352.
34. Sivils JC, I Gonzalez and LJ Bain. (2010). Mice lacking Mrp1 have reduced testicular steroid hormone levels and alterations in steroid biosynthetic enzymes. Gen Comp Endocrinol 167:51–59.
35. Morgan JA, SB Cheepala, Y Wang, G Neale, M Adachi, D Nachagari, M Leggas, W Zhao, K Boyd, et al. (2012). Deregulated hepatic metabolism exacerbates impaired testosterone production in Mrp4-deficient mice. J Biol Chem 287:14456–14466.
36. Mailleux AA, M Overholtzer and JS Brugge. (2008). Lumen formation during mammary epithelial morphogenesis: insights from in vitro and in vivo models. Cell Cycle 7:57–62.
37. Luo W, M Rodriguez, JM Valdez, X Zhu, K Tan, D Li, S Siwko, L Xin and M Liu. (2013). Lgr4 is a key regulator of prostate development and prostate stem cell differentiation. Stem Cells 31:2492–2505.
38. Strouse JJ, I Ivnitski-Steele, A Waller, SM Young, D Perez, AM Evangelisti, O Ursu, CG Bologa, MB Carter, et al. (2013). Fluorescent substrates for flow cytometric evaluation of efflux inhibition in ABCB1, ABCC1, and ABCG2 transporters. Anal Biochem 437:77–87.
39. Jonker JW, J Freeman, E Bolscher, S Musters, AJ Alvi, I Titley, AH Schinkel and TC Dale. (2005). Contribution of the ABC transporters Bcrp1 and Mdr1a/1b to the side population phenotype in mammary gland and bone marrow of mice. Stem Cells 23:1059–1065.
40. Sugimura Y, GR Cunha and AA Donjacour. (1986). Morphological and histological study of castration-induced degeneration and androgen-induced regeneration in the mouse prostate. Biol Reprod 34:973–983.
41. Wang GM, B Kovalenko, EL Wilson and D Moscatelli. (2007). Vascular density is highest in the proximal region of the mouse prostate. Prostate 67:968–975.
42. Vlaming ML, JS Lagas and AH Schinkel. (2009). Physiological and pharmacological roles of ABCG2 (BCRP): recent findings in Abcg2 knockout mice. Adv Drug Deliv Rev 61:14–25.
43. Krishnamurthy P and JD Schuetz. (2011). The role of ABCG2 and ABCB6 in porphyrin metabolism and cell survival. Curr Pharm Biotechnol 12:647–655.
44. Lin YH, HM Chang, FP Chang, CR Shen, CL Liu, WY Mao, CC Lin, HS Lee and CN Shen. (2013). Protoporphyrin IX accumulation disrupts mitochondrial dynamics and function in ABCG2-deficient hepatocytes. FEBS Lett 587:3202–3209.
45. Zhou S, Y Zong, PA Ney, G Nair, CF Stewart and BP Sorrentino. (2005). Increased expression of the Abcg2 transporter during erythroid maturation plays a role in decreasing cellular protoporphyrin IX levels. Blood 105:2571–2576.
46. Brechbuhl HM, N Gould, R Kachadourian, WR Riekhof, DR Voelker and BJ Day. (2010). Glutathione transport is a unique function of the ATP-binding cassette protein ABCG2. J Biol Chem 285:16582–16587.
47. Watson WH, Y Chen and DP Jones. (2003). Redox state of glutathione and thioredoxin in differentiation and apoptosis. BioFactors 17:307–314.
48. Smith J, E Ladi, M Mayer-Proschel and M Noble. (2000). Redox state is a central modulator of the balance between self-renewal and differentiation in a dividing glial precursor cell. Proc Natl Acad Sci U S A 97:10032–10037.
49. Ito K and T Suda. (2014). Metabolic requirements for the maintenance of self-renewing stem cells. Nature reviews. Mol Cell Biol 15:243–256.
50. Wang K, T Zhang, Q Dong, EC Nice, C Huang and Y Wei. (2013). Redox homeostasis: the linchpin in stem cell self-renewal and differentiation. Cell Death Dis 4:e537.
51. Tam NN, Y Gao, YK Leung and SM Ho. (2003). Androgenic regulation of oxidative stress in the rat prostate: involvement of NAD(P)H oxidases and antioxidant defense machinery during prostatic involution and regrowth. Am J Pathol 163:2513–2522.
52. Keppler D, I Leier and G Jedlitschky. (1997). Transport of glutathione conjugates and glucuronides by the multidrug resistance proteins MRP1 and MRP2. Biol Chem 378:787–791.
53. Cole SP and RG Deeley. (2006). Transport of glutathione and glutathione conjugates by MRP1. Trends Pharmacol Sci 27:438–446.
54. Chen ZS, RW Robey, MG Belinsky, I Shchaveleva, XQ Ren, Y Sugimoto, DD Ross, SE Bates and GD Kruh. (2003). Transport of methotrexate, methotrexate polyglutamates, and 17beta-estradiol 17-(beta-D-glucuronide) by ABCG2: effects of acquired mutations at R482 on methotrexate transport. Cancer Res 63:4048–4054.
55. Suzuki M, H Suzuki, Y Sugimoto and Y Sugiyama. (2003). ABCG2 transports sulfated conjugates of steroids and xenobiotics. J Biol Chem 278:22644–22649.

56. van de Wetering K and S Sapthu. (2012). ABCG2 functions as a general phytoestrogen sulfate transporter in vivo. FASEB J 26:4014–4024.
57. Van Brussel JP, G Jan Van Steenbrugge, C Van Krimpen, JF Bogdanowicz, TH Van Der Kwast, FH Schroder and GH Mickisch. (2001). Expression of multidrug resistance related proteins and proliferative activity is increased in advanced clinical prostate cancer. J Urol 165:130–135.
58. Rane JK, D Pellacani and NJ Maitland. (2012). Advanced prostate cancer—a case for adjuvant differentiation therapy. Nat Rev Urol 9:595–602.

Address correspondence to:
Wendy J. Huss
Roswell Park Cancer Institute
Department of Pharmacology and Therapeutics
Elm and Carlton Streets
Buffalo, NY 14263

E-mail: wendy.huss@roswellpark.org

Received for publication June 16, 2014
Accepted after revision January 6, 2015
Prepublished on Liebert Instant Online January 8, 2015